Applied Catalysis B: Environmental 140–141 (2013) 552–558

Contents lists available at SciVerse ScienceDirect

Applied Catalysis B: Environmental

journal homepage: www.elsevier.com/locate/apcatb

Electrostatic self-assembly of platinum nanochains on carbon nanotubes: A highly active electrocatalyst for the oxygen reduction reaction

Yu Chen [1], Jiangfeng Xu [1], Xinyu Liu, Yawen Tang*, Tianhong Lu

Jiangsu Key Laboratory of New Power Batteries, Laboratory of Electrochemistry, College of Chemistry and Materials Science, Nanjing Normal University, 1# Wenyuan Road, Nanjing 210046, PR China

ARTICLE INFO

Article history:
Received 7 December 2012
Received in revised form 20 April 2013
Accepted 25 April 2013
Available online 4 May 2013

Keywords:
Self-sssembly
Platinum nanochains
Carbon nanotubes
Oxygen reduction reaction
Electrocatalytic activity

ABSTRACT

We design and synthesize a multiwalled carbon nanotubes (MWCNTs) supported platinum nanochains (Pt-NCs) catalyst (Pt-NCs/MWCNTs) through the electrostatic self-assembly between phosphonate functionalized Pt-NCs and polyallylamine (PAH) functionalized MWCNTs. The grown mechanism, morphology, structure, and composition of the Pt-NCs are investigated by ultraviolet–visible (UV–vis), transmission electron microscopy (TEM), X-ray diffraction (XRD), X-ray photoelectron spectroscopy (XPS) and zeta potential analysis. XPS and elemental maps measurements confirm the successful immobilization of PAH on the MWCNTs surface. The resultant Pt-NCs/MWCNTs catalyst exhibits better electrocatalytic activity for the oxygen reduction reaction (ORR) than the commercial Pt/C catalyst due to the unique structure and low hydroxyl surface coverage.

1. Introduction

Proton exchange membrane fuel cells (PEMFCs) have attracted more and more attention due to their low emissions of pollutants, high power density, high energy conversion efficiency and low operation temperature [1–6]. However, the high cost of Pt metal and the slow kinetics of the oxygen reduction reaction (ORR) hinder the commercial viability of the PEMFCs technology [7]. One of the efficient approaches to lower the usage of Pt metal is that it is loaded on support, which effectively reduces particle size of Pt nanoparticles [8–12]. Due to the high surface area, excellent chemical stability and high electronic conductibility, carbon nanotubes (CNTs) are considered as potential competitive candidates for catalyst supports [13–18,5]. Moreover, the interaction between Pt nanoparticles and CNTs also improve the ORR activity of Pt [19–22]. Thus, CNTs may provide solid fundamentals for their potential applications in fuel cells.

As we know, the performance of catalysts not only depends on the support material, but also relates to the morphology of Pt nanoparticles [23]. Recently, a lot of investigations have demonstrated the one-dimensional (1D) Pt nanostructures such as nanowires and nanochains that show superior electrocatalytic activity and stability for the ORR due to the enrichment of the low energy facets with high activity and the lager surface area [24–27]. However, the synthesis of 1D Pt nanostructures generally requires the harsh reducing conditions or complicated multistep process. For instance, Song et al. synthesized Pt nanochains in the presence of a soft template formed by cetyltrimethylammonium bromide in a two-phase water–chloroform system [28]. Yu and co-workers synthesized Pt nanowires by using ultrathin Te nanowires as sacrificial templet [26]. At present, Pt/CNTs nanocomposites have been prepared by various methods. However, the morphology of the Pt nanoparticles has lacked control (i.e., they are always sphericity). The electrostatic self-assembly technology, which is based on the surface charge reversal after functionalized each other by polymer wrapping, can solve this problem [29–31]. By merging the technique, Pt nanostructures with a hoping shape can easily deposit on the CNTs surface.

In this work, the phosphonate functionalized Pt nanochains (Pt-NCs) are synthesized through thermal decomposition method at relatively low temperature using platinum(II)-complex as reaction precursor in absence of surfactants and templates. Polyallylamine (PAH) functionalized multiwalled CNTs (MWCNTs) are achieved by the donor–acceptor interaction between PAH and MWCNTs [30,32]. Based on the electrostatic interaction, the Pt-NCs successfully self-assemble on the MWCNTs surface. Electrochemical measurements show that the ORR activity of the Pt-NCs/MWCNTs is much higher than that of the commercial Pt/C catalyst.

* Corresponding author. Tel.: +86 25 85891651; fax: +86 25 83243286.
E-mail address: tangyawen@njnu.edu.cn (Y. Tang).
[1] Both authors contributed equally to this work.

0926-3373/$ – see front matter © 2013 Elsevier B.V. All rights reserved.
http://dx.doi.org/10.1016/j.apcatb.2013.04.049

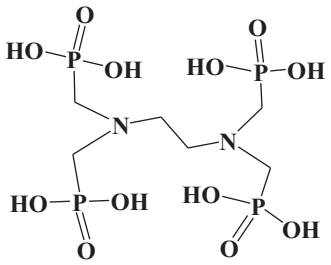

Scheme 1. Structure of ethylenediamine-tetramethylene phosphonic acid (EDTMP).

2. Experimental

2.1. Materials

MWCNTs (>95% purity; outer diameter 20–30 nm; length 10–30 μm; surface area: 110 $m^2\ g^{-1}$) used in this study were purchased from Chengdu Organic Chemicals Co. Ltd., Chinese Academy of Sciences. Ethylenediamine-tetramethylene phosphonic acid (EDTMP, shown in Scheme 1) was purchased from Shandong Taihe Water Treatment Co., Ltd. (Shandong, China). Potassium tetrachloroplatinate(II) (K_2PtCl_4), sodium hydroxide (NaOH) and hydrochloric acid (HCl) were purchased from Sinopharm Chemical Reagent Co., Ltd. (Shanghai, China). The solution pH was adjusted by the addition of dilute NaOH or HCl solution. The commercial 20 wt.% Pt/C catalyst was purchased from E-TEK Division, PEMEAS Fuel Cell Technologies. All the aqueous solutions were prepared with Millipore water having a resistivity of 18.2 MΩ.

2.2. Preparation of PAH functionalized MWCNTs (PAH-MWCNTs)

PAH functionalized MWCNTs were prepared according to a reported method [19,32]. 60 mg MWCNTs were dispersed in 100 mL of 0.5 wt.% PAH aqueous solution containing 1 g KNO_3 by combination of sonication and rapid stirring for 24 h. Then, the supernatant solution was filtered with polycarbonate membrane, and washed several times with Millipore water to remove free polyelectrolyte. After drying at 50 °C for 12 h in a vacuum oven, the PAH-MWCNTs were obtained.

2.3. Preparation of phosphonate functionalized platinum nanochains (Pt-NCs)

In a typical synthesis, 1 mL of 0.0482 mol L^{-1} K_2PtCl_4 and 1 mL of 0.0482 mol L^{-1} EDTMP were added in 18 mL deionized water, and the solution pH was adjusted to 10. After heating at 60 °C for 48 h, the phosphonate functionalized Pt-NCs suspension were obtained.

2.4. Preparation of MWCNTs supported Pt-NCs catalyst (Pt-NCs/MWCNTs)

In a typical procedure, the PAH-MWCNTs were added to the above phosphonate functionalized Pt-NCs suspension and stirred for 14 h. After filtration, wash and dryness, the Pt-NCs/MWCNTs with 20 wt.% Pt was obtained.

2.5. Physical characterizations

Transmission electron microscopy (TEM) measurements were made on a JEOL 2000 transmission electron microscopy operated at an accelerating voltage of 200 kV. Scanning transmission electron microscopy (STEM) and elemental maps were carried out under the high-angle annular bright field mode. X-ray diffraction (XRD) patterns were obtained with Model D/max-rC X-ray diffractometer using Cu Kα radiation source (λ = 1.5406 Å) and operating at 40 kV and 100 mA. X-ray photoelectron spectroscopy (XPS) measurements were performed with a Thermo VG Scientific ESCALAB 250 spectrometer with a monochromatic Al Kα X-ray source (1486.6 eV photons), and the vacuum in the analysis chamber was maintained at about 10^{-9} mbar. The binding energy was calibrated by means of the C1s peak energy of 284.6 eV. The zeta potential measurements were performed with a Malvern Zetasizer Nano ZS90 analyzer at room temperature. Ultraviolet–visible (UV–vis) spectra were recorded at room temperature on a UV3600 spectrophotometer equipped with 1.0 cm quartz cells. Raman spectra of carbon materials were examined with Labram HR 800 UV Raman spectrometer, equipped with a confocal microscope and an Ar ion laser (λ = 514.5 nm).

2.6. Electrochemical measurements

All electrochemical experiments were carried out on a CHI 660C electrochemical workstation (CH Instruments, Shanghai, Chenghua Co.). A standard three-electrode system was used for all electrochemical experiments assembled with a platinum wire as the auxiliary electrode, a saturated calomel electrode protected by Luggin capillary with KCl solution as the reference electrode, and a catalyst modified glassy carbon electrode as the working electrode. Rotating disk electrode test was performed on Gamry's Rotating Disk Electrode (RDE710) with a glassy carbon disk (5 mm diameter). All potentials in this study were reported with respect to the reversible hydrogen electrode (RHE). All of the electrochemical measurements were carried out at 30 °C.

Prior to electrochemical test, the Pt-NCs/MWCNTs were treated with UV irradiation (wavelength at 185 and 254 nm in air for 6 h) to remove the capping agent [33]. The working electrode was prepared according to a reported method [34]. 10 mg Pt-NCs/MWCNTs were mixed in 5 mL of aqueous solution containing 1 mL of iso-propanol and 25 μL of a 5 wt.% Nafion solution (V_{water}:$V_{2\text{-propanol}}$:$V_{5\%Nafion}$ = 0.8:0.2:0.005) and sonicated for 30 min to generate an evenly distributed suspension. Then 25.0 μL of the resulting suspension was laid on the surface of the pre-cleaned glassy carbon electrode (5 mm in diameter) and dried for 30 min before the measurements. The platinum metal loading on the electrode surface was about 10 μg.

All modified electrodes were further pretreated by cycling the potential between −0.2 and 1.2 V for 50 cycles in order to remove any surface contamination prior to electrochemical test [35]. Cyclic voltammetry (CV) measurements were conducted in N_2-saturated 0.1 mol L^{-1} $HClO_4$ aqueous solution. For the oxygen reduction reaction (ORR) measurements, linear sweep voltammograms (LSVs) were conducted in O_2-saturated 0.1 mol L^{-1} $HClO_4$ aqueous solution. The polarization curves were obtained by sweeping the potential from 1.05 to 0.05 V vs. RHE at the scan rate of 5 mV s^{-1} and rotation rate of 1600 rpm.

3. Results and discussion

3.1. Synthesis and characterization of the phosphate functionalized Pt-NCs

UV–vis absorption spectra is a power tool for monitoring the nucleation mechanism and growth processes of Pt nanocrystals [36]. For the reduction method synthesizing noble metal NCs, the initial nucleation involving the reduction of precursor compounds and the subsequent aggregation can be summarized as indirect intermediate complex nucleation pathway and direct nucleation pathway [36]. In the initial stage of the reaction, the absorption

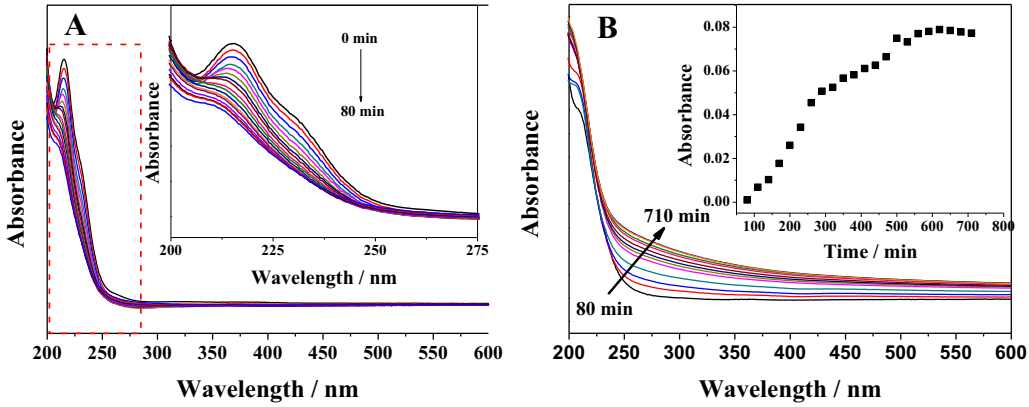

Fig. 1. Time-dependent UV–vis absorption spectra of a mixed solution containing 0.0482 mol L^{-1} K_2PtCl_4 and 0.0482 mol L^{-1} EDTMP (pH 10.0) at 60 °C. The spectra are recorded at a time interval of (A) 5 min and (B) 30 min. Inset in (B) shows dependence of the absorbance value at 500 nm on time.

peak of K_2PtCl_4 at 215 nm originated from the metal-to-ligand (Pt–Cl) charger transfer decreases with increasing time (Fig. 1A). At 80 min, the absorption peak of K_2PtCl_4 completely disappears, indicating that EDTMP has completely interacted with K_2PtCl_4 to generate the EDTMP-Pt^{II} complex due to the strong coordinating capability of EDTMP (Fig. 1A). With further increasing time, a very wide UV absorption in the wavelength range of 800–200 nm appears (Fig. 1B), which is derived from the localized surface plasmon resonance of Pt nanoparticles [37,38]. Insert in Fig. 1B shows the dependence of the absorbance value at 500 nm on time. As observed, the absorbance no longer changes at about 600 min, indicating that the thermal decomposition of EDTMP-Pt^{II} complex has completed [39]. During the thermal decomposition, the UV–vis spectra display a monotonic transition from the initial precursor to final Pt nanoparticles with the reaction time, without the appearance of any additional peaks. This fact indicates no 'Pt_nCl_x' complex [36] generates in the course of initial nucleation, which is attributed to the formation of EDTMP/Pt^{II} complex in the initial reaction stage.

Pt^{II} and Pt^{IV} compounds, such as K_2PtCl_4 and H_2PtCl_6, are commonly used as precursors in the synthesis of Pt nanostructures. Compared to the H_2PtCl_6, there are intrinsic merits for using K_2PtCl_4 as precursors. Obviously, only two electrons are needed to reduce Pt^{II} to Pt^0 while four electrons are required for Pt^{IV}, so the energy using to switch from Pt^{IV} to Pt^{II} for the synthesis of Pt nanostructures can be saved [40]. Meanwhile, the standard electrode potential of $PtCl_4^{2-}/Pt^0$ (0.755 V) is higher than that of $PtCl_6^{2-}/Pt^0$ (0.717 V). According to thermodynamic view, the reduction of K_2PtCl_4 is much easier than that of H_2PtCl_6, which may result in the generation of the Pt nanostructures at relatively low temperature by using K_2PtCl_4 as precursor. In fact, in our previous works, we have successfully synthesized Pt nanoclusters by using EDTMP/Pt^{IV} complex as precursor at a high reaction temperature (120 °C) [39]. Compared to previous report [39], the present synthesis process is simple and lower energy consumption (i.e., the lower reaction temperature, 60 °C), in consistent with thermodynamic prediction.

Fig. 2A is a low magnification TEM image of as-prepared Pt nanostructures. As observed, the as-prepared Pt nanostructures are nanochains and the average cross-sectional diameter is about 3.5 ± 0.5 nm. Further high resolution TEM (HR-TEM) image shows that the Pt-NCs are composed of several single-crystalline elongated primary nanoparticles (Fig. 2B). These nanoparticles are interconnected in a head-to-head manner via various angles to form the nanochains. Since UV–vis measurements have demonstrated that no 'Pt_nCl_x' complex [36] generates in the course of initial nucleation, the oriented attachment grown mechanism [41,42] is responsible for the formation of the nanochains. HR-TEM image shows that the *d*-spacing of adjacent fringes for the Pt-NCs is 0.2286 nm (Fig. 2B), corresponding to the (1 1 1) interplanar distance of face centered cubic (*fcc*) Pt. It is worth noting that fringes are discontinuous, confirming the oriented attachment grown mechanism.

The surface composition of the Pt-NCs is investigated by XPS measurement. Fig. 3A is the spectra of the Pt-NCs in the N1s and P2p

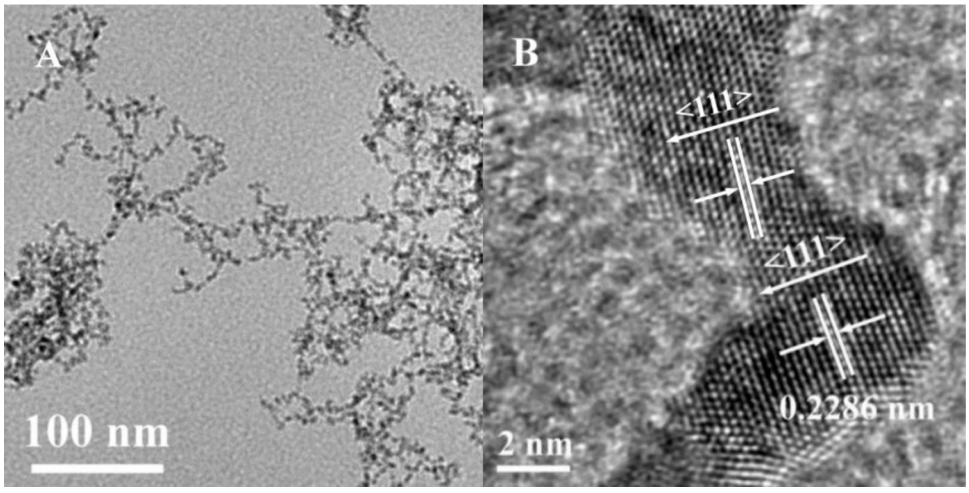

Fig. 2. (A) TEM and (B) HR-TEM images of the Pt-NCs.

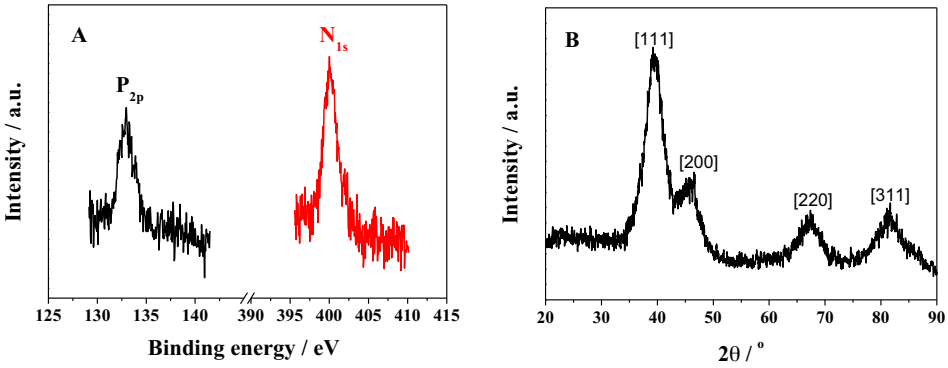

Fig. 3. (A) XPS spectra of the Pt-NCs in the N1s and P2p regions. (B) XRD pattern of the Pt-NCs.

regions. The appearance of N1s (400.0 eV) and P2p peaks (133.0 eV) indicates that some aminophosphonate molecules adsorb on the Pt-NCs surface [39]. The zeta potential of the Pt-NCs is -37 ± 5 mV at pH 7.0, indicating that the negatively charged phosphonic acid groups are exposed to the outside of the Pt-NCs. These results confirm that phosphate functionalized Pt-NCs are successfully synthesized. The crystalline nature of the Pt-NCs was confirmed by XRD (Fig. 3B). Well-resolved diffraction peaks at 2θ values of 39.4°, 46.6°, 67.5° and 81.5° are indexed as Pt(1 1 1), Pt(2 0 0), Pt(2 2 0) and Pt(3 1 1) diffraction peaks, indicating that Pt-NCs possess the *fcc* structure. According to Scherrer equation, the average size of the Pt-NCs is calculated to be 3.2 nm, in good agreement with the TEM result.

3.2. Synthesis and characterization of the PAH-MWCNTs

PAH is a positively charged polyelectrolyte [43], which can irreversibly adsorb onto the MWCNTs surface via the donor–acceptor interaction between PAH and MWCNTs [30,32]. Fig. 4 shows the XPS spectrum of the PAH-MWCNTs in N1s region. Three discernible N1s peaks locate at 399.8, 401.7 and 407.0 eV (denoted as Na, Nb and Nc), respectively. The appearance of N1s peak confirms that PAH molecules have successfully wrapped on MWCNTs. The Na and Nb peaks originate from uncharged ($-NH_2$) and charged nitrogen atoms ($-NH_3^+$), respectively [30,44–46]. The Nc peak may be attributed to physisorbed nitrogen [47].

Fig. 5 shows a representative high-angle annular bright-field scanning TEM (HAABF-TEM) image and the corresponding energy dispersive X-ray (EDX) maps for C and N elements of an individual PAH-MWCNTs. As observed, the N element is distributed evenly in whole MWCNTs, indicating the uniform distribution of PAH on the MWCNTs surface.

The surface charge of the PAH-MWCNTs was characterized by zeta potential. The zeta potential of the as-prepared PAH-MWCNTs

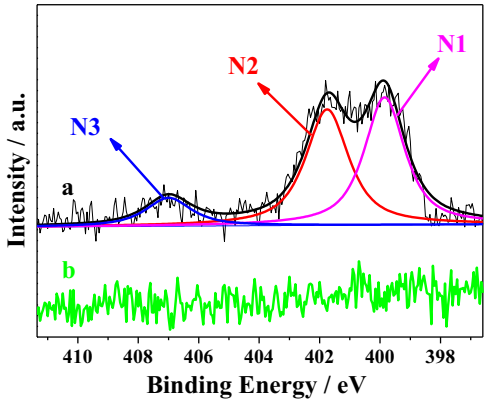

Fig. 4. XPS spectrum of (a) the PAH-MWCNTs and (b) pristine MWCNTs in N1s region.

suspension is 25 ± 5 mV at pH 7.0. The electrostatic repulsion between charged amine groups, the bulky molecule size of PAH, and excellent hydrophilic property of amine groups can facilitate the solubility of PAH-MWCNTs [19]. As respected, the PAH-MWCNTs are soluble in water with good storage stability at ambient temperature (Fig. 6a). No precipitation or flocculation is observed even after three months (data not shown). For comparison, the dispersion of the pristine MWCNTs in water is difficult, even with the help of sonication (Fig. 6b). Obviously, the good solubility of the PAH-MWCNTs facilitates the immobilization of the Pt-NCs on the MWCNTs via electrostatic self-assembly.

In general, non-covalent functionalization of the MWCNTs effectively preserves the atomic and electronic structures of the MWCNTs compared to the chemical modification of the MWCNTs [48]. Fig. 7 shows the Raman spectra of the pristine MWCNTs and PAH-MWCNTs. Both of them exhibit two characteristic

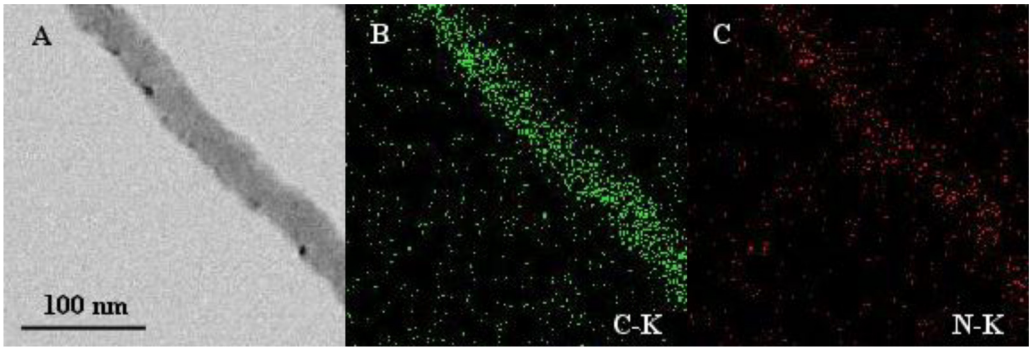

Fig. 5. (A) HAABF-TEM image and elemental maps for (B) C and (C) N elements of the PAH-MWCNTs.

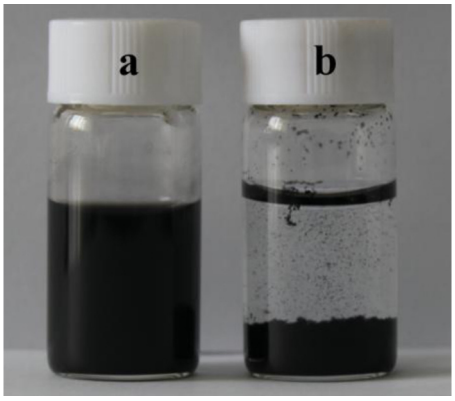

Fig. 6. Digital photographs of (a) the PAH-MWCNTs and (b) pristine MWCNTs dispersed in water for 30 min.

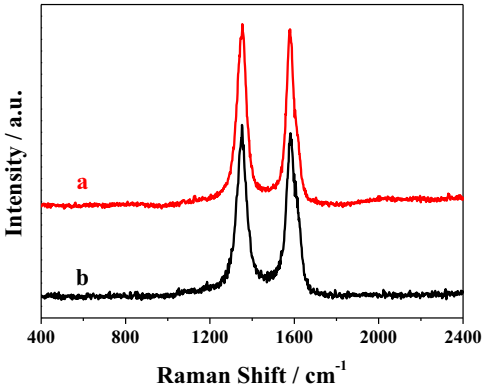

Fig. 7. Raman spectra of (a) the PAH-MWCNTs and (b) pristine MWCNTs.

peaks at 1350.27 and 1583.86 cm^{-1}, corresponding to the D band and G band, respectively. The intensity ratio of the D band to G band of the MWCNTs, denoted as I_D/I_G, directly indicates the structural changes of the MWCNTs [49]. The I_D/I_G ratios of the pristine MWCNTs and PAH-MWCNTs are 1.05 and 1.02, respectively. This result indicates that the atomic and electronic structures of MWCNTs have no change after PAH functionalization, which is in favor of electron transfer in electrochemical reaction.

3.3. Interaction between Pt-NCs and MWCNTs

Based on the mechanism of electrostatic self-assembly, the PAH-MWCNTs can easily bind the Pt-NCs because of the electrostatic interaction and/or hydrogen bond between amine groups and phosphonic acid groups [50–53]. Fig. 8A shows the TEM image of the Pt-NCs/MWCNTs. It is observed that the Pt-NCs have uniform dispersion on the PAH-MWCNTs surface with no agglomeration. In contrast, the Pt-NCs deposited on the pristine MWNTs are found randomly dispersed with aggregation (Fig. S1). The uniform distribution of PAH on the MWCNTs surface and the strong interaction between amine groups and phosphonic acid groups are responsible for the uniform attachment of the Pt-NCs on the MWCNTs surface. Further HR-TEM image shows the shape of the Pt-NCs still preserve, indicating the interaction between MWCNTs and Pt-NCs does not change the methodology of the Pt-NCs.

3.4. Oxygen reduction reaction (ORR) on Pt-NCs/MWCNTs catalyst

Fig. 9A shows cyclic voltammetry (CV) curves of the Pt-NCs/MWCNTs and commercial E-TEK Pt/C in N_2-saturated 0.1 mol L^{-1} $HClO_4$ solution at 50 mV s^{-1}. The electrochemically active surface area (ECSA) of catalyst was calculated by measuring the charge collected in the hydrogen adsorption/desorption region and assuming a value of 210 μC cm^{-2} for the adsorption of a hydrogen monolayer [54]. ECSA value for the Pt-NCs/MWCNTs (54.3 m^2 g^{-1}) is lower than that of commercial E-TEK Pt/C (61.8 m^2 g^{-1}), which is ascribed to the difference of particle size (Fig. S2). Meanwhile, it is worth noting that onset oxidation potential of the Pt-NCs/MWCNTs has a positive shifts in comparison with commercial E-TEK Pt/C, suggesting that the Pt-NCs/MWCNTs have the weaker oxophilicity than commercial E-TEK Pt/C. Fig. 9B clearly shows that the Pt-NCs/MWCNTs have the lower hydroxyl surface coverage (Θ_{OH}) than commercial E-TEK Pt/C, confirming that the weaker adsorption of hydroxyl species on Pt-NCs/MWCNTs surface, in consist with the CV observation.

The electrocatalytic activity of the Pt-NCs/MWCNTs were measured using a rotating-disk electrode (RDE) operated at 1600 rpm in O_2-saturated 0.1 mol L^{-1} $HClO_4$ solution (Fig. 10A). The current density was normalized in reference to the geometrical area of the glassy carbon electrode. The onset ORR potential is more positive for the Pt-NCs/MWCNTs (at ca. 0.881 V) than E-TEK Pt/C (at ca. 0.870 V). Although ECSA of Pt-NCs/MWCNTs is lower than that of commercial E-TEK Pt/C, the Pt-NCs/MWCNTs have a much

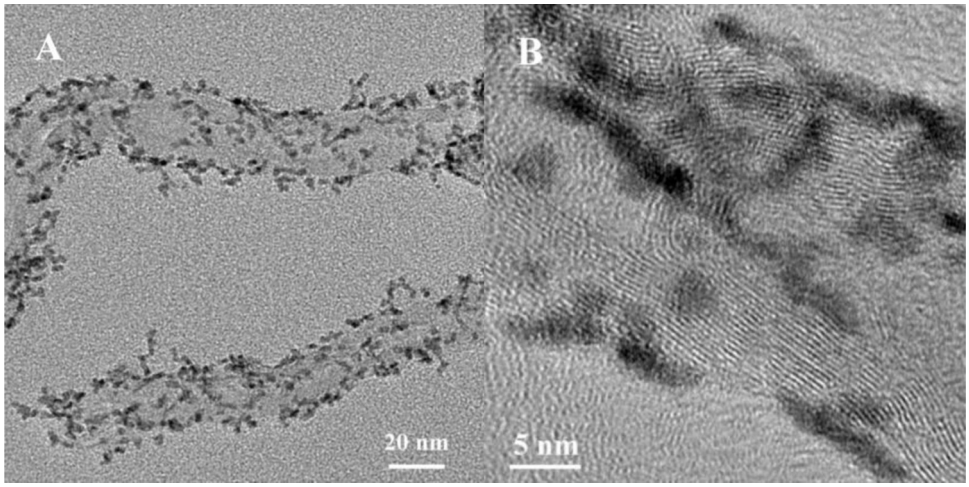

Fig. 8. (A) TEM and (B) HR-TEM images of the Pt-NCs/MWCNTs.

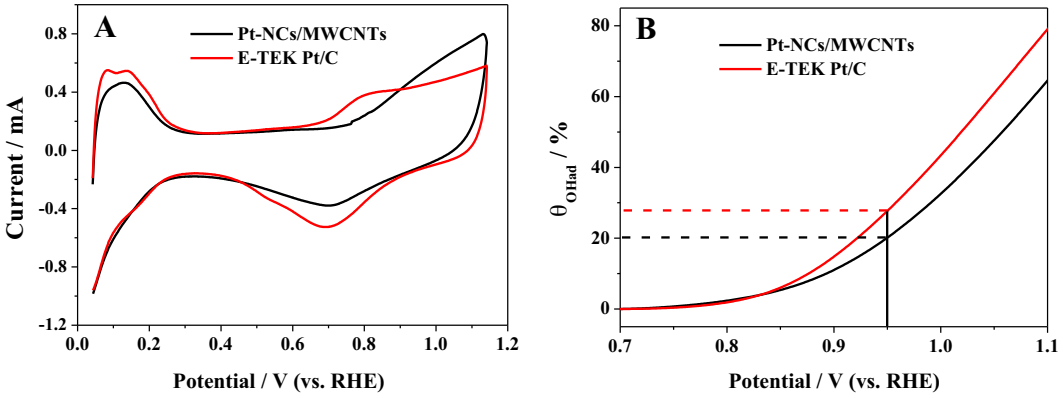

Fig. 9. (A) CV curves for the Pt-NCs/MWCNTs and commercial E-TEK Pt/C in N_2-saturated 0.1 mol L^{-1} $HClO_4$ solution at 50 mV s^{-1}. (B) Hydroxyl surface coverage (Θ_{OH}) for the Pt-NCs/MWCNTs and E-TEK Pt/C.

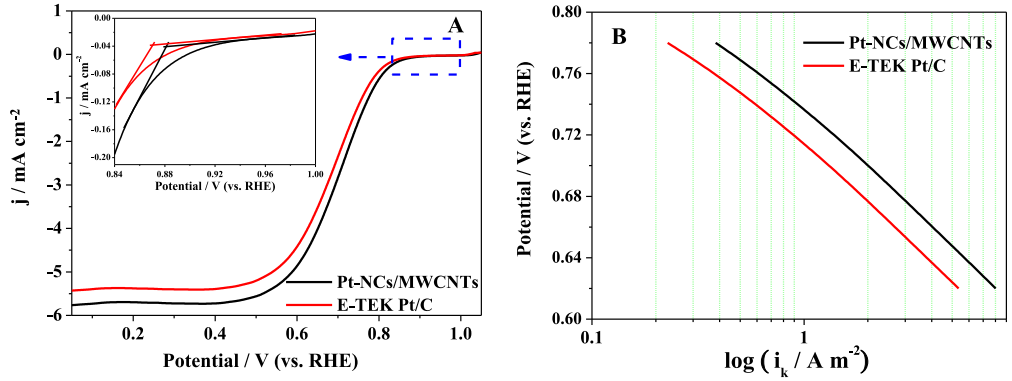

Fig. 10. (A) ORR polarization curves for the Pt-NCs/MWCNTs (black curve) and E-TEK Pt/C (red curve) in O_2-saturated 0.1 mol L^{-1} $HClO_4$ solution at a scan rate of 5 mV s^{-1} and rotation rate of 1600 rpm. (B) Kinetic currents normalized to the electrochemical active surface areas at different potential. (For interpretation of the references to color in this figure legend, the reader is referred to the web version of the article.)

bigger diffusion-limiting current density for ORR than E-TEK Pt/C at 0.05 V (5.76 mA cm^{-2} vs. 5.43 mA cm^{-2}) [54–59]. Likely, three-dimensional network-like architecture of the Pt-NCs/MWCNTs on electrode facilitates mass transport of O_2 at cathode [26]. The kinetic current density (i_k), which represents the intrinsic activity of the catalysts and calculated using Koutecky–Levich equation [34,60], is 2.4 A m^{-2} at 0.7 V for Pt-NCs/MWCNTs, which is 2 times for E-TEK Pt/C catalyst (1.2 A m^{-2}). The enhanced catalytic activity may be correlated with the abundant Pt(1 1 1) facets with low energy and the low hydroxyl species coverage [34,61,62]. In addition, PAH is a proton conducting material, which enhances the electrical conductivity of the PAH-MWCNTs [43,63,64] and consequently improves the ORR kinetics.

4. Conclusions

In summary, we report a simple route to synthesize the phosphonate functionalized Pt-NCs in the absence of any surfactants and templates. By means of the electrostatic interaction, the Pt-NCs successfully self-assemble on the PAH-MWCNTs. The as-synthesized Pt-NCs/MWCNTs exhibit superior electrochemical activity toward ORR compared to commercial Pt/C catalyst, which can be attributed to the following reasons: (i) the uniquely anisotropic nature of the Pt-NCs with abundant low energy crystal facets; (ii) the low hydroxyl surface coverage; (iii) the particularly 3D network-like architecture of Pt-NCs/MWCNTs and (iv) the particular proton conductibility of PAH layers on MWCNTs. With the advantages of enhanced catalytic activity and simple fabrication, the Pt-NCs/MWCNTs synthesized by this strategy will be promising for applications in fuel cells.

Acknowledgments

The authors are grateful for the financial support of National "973" program of China (2012CB215500), NSFC (20873065 and 21073094), the United Fund of NSFC and Yunnan Province (U1137602), Industry-Academia Cooperation Innovation Fund Project of Jiangsu Province (BY2012001), University Postgraduate Research and Innovation Project in Jiangsu Province (CXLX11_0871), and a project funded by the Priority Academic Program Development of Jiangsu Higher Education Institutions.

Appendix A. Supplementary data

Supplementary data associated with this article can be found, in the online version, at http://dx.doi.org/10.1016/j.apcatb.2013.04.049.

References

[1] K. Sasaki, H. Naohara, Y. Cai, Y.M. Choi, P. Liu, M.B. Vukmirovic, J.X. Wang, R.R. Adzic, Angewandte Chemie International Edition 49 (2010) 8602–8607.
[2] B. Avasarala, T. Murray, W. Li, P. Haldar, Journal of Materials Chemistry 19 (2009) 1803–1805.
[3] J. Lu, H. Tang, S. Lu, H. Wu, S.P. Jiang, Journal of Materials Chemistry 21 (2011) 6668–6676.
[4] Y. Huang, J. Cai, Y. Guo, Applied Catalysis B: Environmental 129 (2013) 549–555.
[5] Z.Z. Jiang, Z.B. Wang, W.L. Qu, D.M. Gu, G.P. Yin, Applied Catalysis B: Environmental 123–124 (2012) 214–220.
[6] G.J. Zhang, Y.N. Wang, X. Wang, Y. Chen, Y.M. Zhou, Y.W. Tang, L.D. Lu, J.C. Bao, T.H. Lu, Applied Catalysis B: Environmental 102 (2011) 614–619.
[7] P. Hernandez, M. Montiel, P. Ocon, J.L. Gomez, S. Garcia, S. Rojas, J.L.G. Fierro, Applied Catalysis B: Environmental 99 (2010) 343–352.

[8] S.Y. Huang, P. Ganesan, B.N. Popov, Applied Catalysis B: Environmental 96 (2010) 224–231.
[9] Y. Wang, S.Q. Song, V. Maragou, P.K. Shen, P. Tsiakaras, Applied Catalysis B: Environmental 89 (2009) 223–228.
[10] N. Elezovic, B. Babic, P. Ercius, V. Radmilovic, L.M. Vracar, N. Krstajic, Applied Catalysis B: Environmental 125 (2012) 390–397.
[11] D.P. He, Y.L. Jiang, H.F. Lv, M. Pan, S.C. Mu, Applied Catalysis B: Environmental 132 (2013) 379–388.
[12] D. Sebastian, A.G. Ruiz, I. Suelves, R. Moliner, M.J. Lazaro, V. Baglio, A. Stassi, A.S. Arico, Applied Catalysis B: Environmental 115 (2012) 269–275.
[13] K.W. Park, B.K. Kwon, J.H. Choi, I.S. Park, Y.M. Kim, Y.E. Sung, Journal of Power Sources 109 (2002) 439–445.
[14] Y. Chen, G. Zhang, J. Ma, Y. Zhou, Y. Tang, T. Lu, International Journal of Hydrogen Energy 35 (2010) 10109–10117.
[15] P. Li, H. Liu, Y. Ding, Y. Wang, Y. Chen, Y. Zhou, Y. Tang, H. Wei, C. Cai, T. Lu, Journal of Materials Chemistry 22 (2012) 15370–15378.
[16] M. Zheng, P. Li, G. Fu, Y. Chen, Y. Zhou, Y. Tang, T. Lu, Applied Catalysis B: Environmental 129 (2013) 394–402.
[17] K. Wu, X. Mao, Y. Liang, Y. Chen, Y. Tang, Y. Zhou, J. Lin, C. Ma, T. Lu, Journal of Power Sources 219 (2012) 258–262.
[18] X. Yang, J. Zheng, M. Zhen, X. Meng, F. Jiang, T. Wang, C. Shu, L. Jiang, C. Wang, Applied Catalysis B: Environmental 121–122 (2012) 57–64.
[19] S. Zhang, Y. Shao, G. Yin, Y. Lin, Journal of Materials Chemistry 20 (2010) 2826–2830.
[20] S. Wang, S.P. Jiang, T.J. White, J. Guo, X. Wang, The Journal of Physical Chemistry C 113 (2009) 18935–18945.
[21] F. Hasche, M. Oezaslan, P. Strasser, Physical Chemistry Chemical Physics 12 (2010) 15251–15258.
[22] L. Zhang, L. Wang, C.M.B. Holt, B. Zahiri, Z. Li, K. Malek, T. Navessin, M.H. Eikerling, D. Mitlin, Energy & Environmental Science 5 (2012) 6156–6172.
[23] M.R. Kim, D.K. Lee, D.J. Jang, Applied Catalysis B: Environmental 103 (2011) 253–260.
[24] S.V.N.T. Kuchibhatla, A. Karakoti, D. Bera, S. Seal, Progress in Materials Science 52 (2007) 699–913.
[25] C. Koenigsmann, S.S. Wong, Energy & Environmental Science 4 (2011) 1161–1176.
[26] H.W. Liang, X. Cao, F. Zhou, C.H. Cui, W.J. Zhang, S.H. Yu, Advanced Materials 23 (2011) 1467–1471.
[27] S.M. Alia, G. Zhang, D. Kisailus, D. Li, S. Gu, K. Jensen, Y. Yan, Advanced Functional Materials 20 (2010) 3742–3746.
[28] Y. Song, R.M. Garcia, R.M. Dorin, H.R. Wang, Y. Qiu, E.N. Coker, W.A. Steen, J.E. Miller, J.A. Shelnutt, Nano Letters 7 (2007) 3650–3655.
[29] S. Zhang, Y. Shao, G. Yin, Y. Lin, Angewandte Chemie International Edition 49 (2010) 2211–2214.
[30] H. Paloniemi, M. Lukkarinen, T. Aaritalo, S. Areva, J. Leiro, M. Heinonen, K. Haapakka, J. Lukkari, Langmuir 22 (2005) 74–83.
[31] S. Zhang, Y. Shao, G. Yin, Y. Lin, Applied Catalysis B: Environmental 102 (2011) 372–377.
[32] J.H. Rouse, P.T. Lillehei, J. Sanderson, E.J. Siochi, Chemistry of Materials 16 (2004) 3904–3910.
[33] C. Wang, H. Daimon, Y. Lee, J. Kim, S. Sun, Journal of the American Chemical Society 129 (2007) 6974–6975.
[34] Z. Peng, H. Yang, Journal of the American Chemical Society 131 (2009) 7542–7543.
[35] D. Wang, H.L. Xin, Y. Yu, H. Wang, E. Rus, D.A. Muller, H.D. Abruna, Journal of the American Chemical Society 132 (2010) 17664–17666.
[36] T. Yao, S. Liu, Z. Sun, Y. Li, S. He, H. Cheng, Y. Xie, Q. Liu, Y. Jiang, Z. Wu, Z. Pan, W. Yan, S. Wei, Journal of the American Chemical Society 134 (2012) 9410–9416.
[37] N.C. Bigall, T. Hartling, M. Klose, P. Simon, L.M. Eng, A. Eychmuller, Nano Letters 8 (2008) 4588–4592.
[38] Y. Bi, J. Ye, Chemical Communications 46 (2010) 1532–1534.
[39] J. Xu, X. Wu, G. Fu, X. Liu, Y. Chen, Y. Zhou, Y. Tang, T. Lu, Electrochimica Acta 80 (2012) 233–239.
[40] J. Zeng, Y. Ma, U. Jeong, Y. Xia, Journal of Materials Chemistry 20 (2010) 2290–2301.
[41] X. Teng, W.Q. Han, W. Ku, M. Hucker, Angewandte Chemie 120 (2008) 2085–2088.
[42] H. Zheng, R.K. Smith, Y.W. Jun, C. Kisielowski, U. Dahmen, A.P. Alivisatos, Science 324 (2009) 1309–1312.
[43] J. Park, P.T. Hammond, Macromolecules 38 (2005) 10542–10550.
[44] S.W. Won, J. Park, J. Mao, Y.S. Yun, Bioresource Technology 102 (2011) 3888–3893.
[45] N. Li, R. Bai, Industrial & Engineering Chemistry Research 44 (2005) 6692–6700.
[46] C. Liu, R. Bai, L. Hong, Journal of Colloid and Interface Science 303 (2006) 99–108.
[47] N. Soin, S.S. Roy, L. Karlsson, J.A. McLaughlin, Diamond and Related Materials 19 (2010) 595–598.
[48] M. Fagnoni, A. Profumo, D. Merli, D. Dondi, P. Mustarelli, E. Quartarone, Advanced Materials 21 (2009) 1761–1765.
[49] V. Datsyuk, M. Kalyva, K. Papagelis, J. Parthenios, D. Tasis, A. Siokou, I. Kallitsis, C. Galiotis, Carbon 46 (2008) 833–840.
[50] Y. Chen, B. Jin, L.R. Guo, X.J. Yang, W. Chen, G. Gu, L.M. Zheng, X.H. Xia, Chemistry-A European Journal 14 (2008) 10727–10734.
[51] Y. Chen, X.J. Yang, L.R. Guo, J. Li, X.H. Xia, L.M. Zheng, Analytica Chimica Acta 644 (2009) 83–89.
[52] M. Zheng, Y. Zhou, Y. Chen, Y. Tang, T. Lu, Electrochimica Acta 55 (2010) 4789–4798.
[53] F. Zhang, L. Zhang, J. Xing, Y. Tang, Y. Chen, Y. Zhou, T. Lu, X. Xia, ChemPlusChem 77 (2012) 914–922.
[54] B. Lim, M. Jiang, P.H.C. Camargo, E.C. Cho, J. Tao, X. Lu, Y. Zhu, Y. Xia, Science 324 (2009) 1302–1305.
[55] N. Markovic, H. Gasteiger, P.N. Ross, Journal of the Electrochemical Society 144 (1997) 1591–1597.
[56] J. Zhang, Y. Mo, M. Vukmirovic, R. Klie, K. Sasaki, R. Adzic, The Journal of Physical Chemistry B 108 (2004) 10955–10964.
[57] L. Jiang, A. Hsu, D. Chu, R. Chen, Journal of the Electrochemical Society 156 (2009) B370–B376.
[58] L.H. Jiang, A. Hsu, D. Chu, R.R. Chen, Electrochimica Acta 55 (2010) 4506–4511.
[59] S. Chen, W.C. Sheng, N. Yabuuchi, P.J. Ferreira, L.F. Allard, Y. Shao, The Journal of Physical Chemistry C 113 (2008) 1109–1125.
[60] U. Paulus, T. Schmidt, H. Gasteiger, R. Behm, Journal of Electroanalytical Chemistry 495 (2001) 134–145.
[61] Z. Peng, H. Yang, Nano Today 4 (2009) 143–164.
[62] V.R. Stamenkovic, B. Fowler, B.S. Mun, G. Wang, P.N. Ross, C.A. Lucas, N.M. Markovic, Science 315 (2007) 493–497.
[63] W. Li, C. Liang, W. Zhou, J. Qiu, Z. Zhou, G. Sun, Q. Xin, The Journal of Physical Chemistry B 107 (2003) 6292–6299.
[64] J. Choi, M.F. Rubner, Macromolecules 38 (2005) 116–124.